NUCL SCI TECH (2020) 31:83
https://doi.org/10.1007/s41365-020-00790-x

Th–U cycle performance analysis based on molten chloride salt and molten fluoride salt fast reactors

Liao-Yuan He[1,2,3] · Shao-Peng Xia[1,2] · Xue-Mei Zhou[1,2] · Jin-Gen Chen[1,2,3] · Gui-Min Liu[1,2,3] · Yang Zou[1,2,3] · Rui Yan[1,2]

Received: 6 March 2020 / Revised: 28 May 2020 / Accepted: 29 May 2020 / Published online: 8 August 2020

Abstract The recent development of molten salt fast reactors has generated a renewed interest in them. As compared to traditional solid fuel fast neutron systems, it has many unique advantages, e.g., lower fissile inventory, no initial criticality reserve, waste reduction, and a simplified fuel cycle. It has been recognized as an ideal reactor for achieving a closed Th–U cycle. Based on the carrier salt, molten salt fast reactors could be divided into either a molten chloride salt fast reactor (MCFR) or a molten fluoride salt fast reactor (MFFR); to compare their Th–U cycle performance, the neutronic parameters in a breeding and burning (B&B) transition scenario were studied based on similar core geometry and power. The results demonstrated that the required reprocessing rate for an MCFR to achieve self-breeding was lower than that of an MFFR. Moreover, the breeding capability of an MCFR was better than that of an MFFR; at a reprocessing rate of 40 L/day, using LEU and Pu as start-up fissile materials, the doubling time (DT) of an MFFR and MCFR were 88.0 years and 48.0 years, and 16.5 years and 16.2 years, respectively. Besides, an MCFR has lower radio-toxicity due to lower buildup of fission products (FPs) and transuranium (TRU), while an MFFR has a larger, delayed neutron fraction with smaller changes during the entire operation.

Keywords Th–U cycle · Molten salt fast reactor · Breeding capability · Doubling time

1 Introduction

Molten salt fast reactors have generated a growing interest from both scientific and industrial perspectives due to their intrinsic characteristics of sustainability, breeding capability, and safety [1–3]. Firstly, the closed fuel cycle leads to lower radio-toxicity due to a lower actinide inventory. Moreover, owing to the hard energy spectrum, fast reactors have an outstanding breeding capacity and breeding fissile isotopes from fertile nuclides, significantly extending the fuel availability. In addition, atmospheric pressure operation and small residual reactivity greatly improve the safety of the system. Finally, the yield and absorption cross section of fission products are small in the fast spectrum, making online reprocessing less challenging, which is conducive to their deployment. Therefore, molten salt fast reactors have been recognized as ideal reactors for achieving a closed Th–U cycle; they have development potential and research significance.

In general, a molten salt fast reactor could use a fluoride or chloride salt as a fuel carrier salt, corresponding to two reactor types, i.e., a molten fluoride salt fast reactor (MFFR) or a molten chloride salt fast reactor (MCFR). The success of the molten salt reactor experiment (MSRE) led

This work was supported by the Chinese TMSR Strategic Pioneer Science and Technology Project (No. XDA02010000) and the National Natural Science Foundation of China (No. 91326201).

✉ Gui-Min Liu
liuguimin@sinap.ac.cn

✉ Rui Yan
yanrui@sinap.ac.cn

[1] Shanghai Institute of Applied Physics, Chinese Academy of Sciences, Shanghai 201800, China

[2] CAS Innovative Academies in TMSR Energy System, Chinese Academy of Sciences, Shanghai 201800, China

[3] University of Chinese Academy of Sciences, Beijing 100049, China

to a development in an understanding of corrosion as well as related reprocessing technologies of fluoride salt; hence, the MFFR was well developed. For instance, the Molten Salt Actinide Recycler & Transmuter (MOSART) is a typical MFFR [4], designed for TRU incineration by the Kurchatov Institute of Russia within the International Science and Technology Center project 1606 (ISTC#1606). The feasibility of the Th–U cycle for MOSART was recently evaluated; various fuel cycle programs including the converter, iso-breeder, and breeder were researched. Moreover, under the European Evaluation and Viability of Liquid Fuel Fast Reactor System (EVOL), the Centre National de la Recherche Scientifique (CNRS) proposed the molten salt fast reactor (MSFR) [3, 5]. The primary difference in the design of an MSFR versus that of other MSRs is the absence of a graphite moderator from the core; hence, it is a breeder reactor with a fast spectrum. Having unique characteristics (lower fissile inventory, excellent safety coefficients, simplified design, and no requirement for criticality reserve ($k_{\text{eff}} \approx 1.000$)), it was selected for further research by the Generation IV International Forum in 2008 [6].

Although there is no successful operation experience of MCFR, it has obvious advantages as compared to an MFFR which make it worth researching [7, 8]. First, the atomic mass of Cl is bigger than that of F, making the energy spectrum harder in MCFR than in MFFR; therefore, the extraction period of fission products (FPs) can be prolonged due to their smaller neutron absorption cross sections and lower content under a faster spectrum. Importantly, the chloride salt has higher solubility among the actinides; hence, heavier nuclides could be loaded in the chloride salt, which could further contribute to the breeding capability.

Research on MCFR began in the 1950s by Oak Ridge National Laboratory (ORNL), and the design adopted $NaCl + MgCl_2 + PuCl_3 + UCl_3$ as a fissile fuel salt and UO_2 + Na as a solid blanket [7]. A breeding ratio (BR) of 1.09 could be achieved, which demonstrated the practicability of using chlorine salt for fuel breeding in a fast reactor. In the 1960s, the British Atomic Energy Authority carried out research on MCFRs [9], in which $NaCl + UCl_3 + PuCl_3$ was used as a fuel salt and $NaCl + {}^{238}UCl_3$ as a breeding salt; a BR of 1.53 was attainable. The chloride salt fast reactor has been receiving increased attention globally. In Britain, Moltex Energy recently proposed a stable salt fast reactor, a pool-type fast reactor, in which the fuel tube is loaded with chloride fuel; due to good intrinsic safety, it has an enormous economic advantage over other fast reactor designs [10]. In addition, the proposed German dual fluid reactor (DFR) [11] combines the advantages of the MSRE, lead-cooled fast reactor (LFR), and very high-temperature reactor (VHTR) by using two separate fluids; the molten salt of the DFR is cooled by a separate liquid lead loop, which allows for higher power density and better breeding capability. However, most of the above research was on the U–Pu cycle performance of MCFRs; in comparison, the Th–U cycle offers unique advantages: The lower mass number of Th fosters a lower endogenous TRU generation, which yields lower radio-toxicity and decay heat. Hence, it could benefit public acceptance; besides, Th is more abundant than U in nature. Therefore, studying the Th–U cycle performance of an MCFR is of great significance. In the previous work, the breeding capability of an MCFR was optimized [12]. Our work aims to identify neutron properties of the Th–U cycle based on an optimized MCFR and compare it with an MFFR under similar conditions.

2 Calculation model and reprocessing schemes

2.1 Calculation model

Here, the basic core design (Fig. 1) refers to REBUS-3700 [13], which is a typical chloride salt fast reactor designed in France. Table 1 lists the detailed structural parameters. It is a two-fluid MSR with a thermal power of 2500 MW. The active zone consists of a compact cylinder (height/diameter ratio = 1) in which liquid fluoride fuel salt flows from the bottom to the top with no solid moderator. A fertile zone surrounds the active core in both the radial and axial directions (blue area, Fig. 1). Surrounding the fertile salt is a graphite reflector (yellow area, Fig. 1), which is used for saving fertile fuel [14, 15]. Outside the graphite reflector, B_4C (green area, Fig. 1) has been applied to absorb leaking neutrons from the reactor. A Ti-based alloy is used as supporting material on the outermost section. In an MFFR, the composition of the adopted fertile salt and fuel salt is 77.5 mol% LiF–22.5 mol% $(HM)F_4$ in mol%, and the density of both is 4.1 g/cm^3 [2, 16]. In an MCFR, the corresponding composition of both the fertile salt and fuel salt is 55 mol% NaCl–45 mol% $(HM)Cl_4$, and their density is 3.6 g/cm^3 [17]. Note that $(Th + U)Cl_4$ could be soluble to 45 mol% in the chloride salt, and to only 22.5 mol% in LiF, resulting from a higher solubility of actinides in chloride salt.

2.2 Reprocessing schemes

Online molten salt reprocessing is one of the most crucial features of an MSR in comparison with a traditional solid fuel reactor. A diagram of the reprocessing is shown in Fig. 2, which refers to an MSFR [2, 3]. Two key systems exist for the online reprocessing: (1) An He gaseous bubbling system, which continuously removes gaseous and

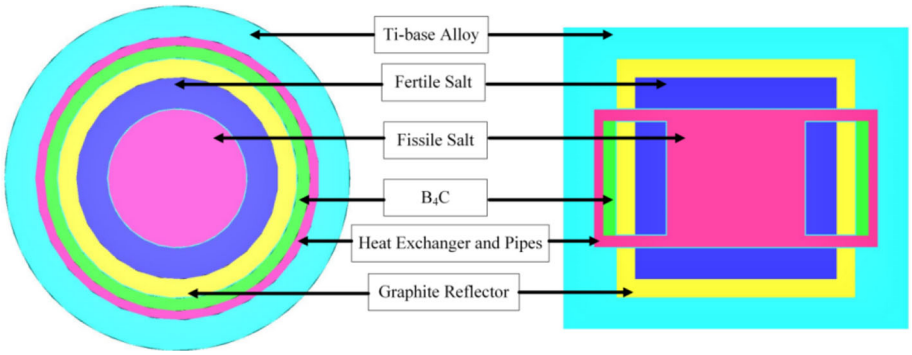

Fig. 1 (Color online) Cross and vertical sections of the calculation model

Table 1 Main parameters of MCFR and MFFR

Parameters	MFFR	MCFR
Thermal power (MW)	2500	2500
Fuel salt (%)	LiF:(HN)F_3 = 77.5:22.5	NaCl:(HN)Cl_3 = 55:45
Fertile salt (%)	LiF:ThF_4 = 77.5:22.5	NaCl:$ThCl_4$ = 55:45
Enrichment of ^{7}Li (%)	100	–
Enrichment of ^{37}Cl (%)	–	100
Temperature of fuel salt (K)	1023	1023
Temperature of fertile salt (K)	973	973
Thermal expansion (K)	− 1.78E−04	− 3.00E−04
Density of graphite (g cm^{-3})	2.3	2.3
Density of B_4C (g cm^{-3})	2.52	2.52
Density of salt (g cm^{-3})	4.1	3.6
Radius of core (cm)	158.5	158.5
Thickness of blanket (cm)	60	60
Thickness of reflector (cm)	45	45
Thickness of B_4C (cm)	35	35

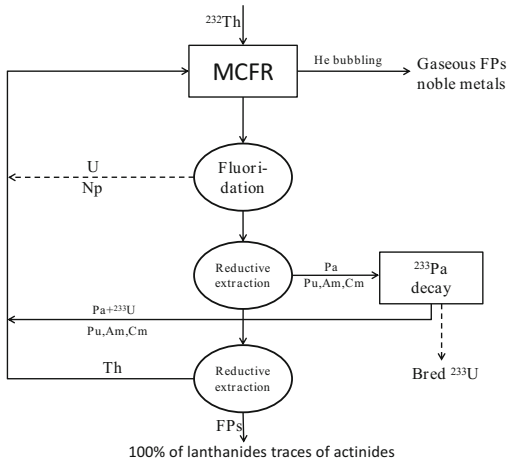

Fig. 2 Reprocessing of the core

non-dissolved FPs (H, He, N, O, Ne, Ar, Kr, Xe, Rn, Zr, Ga, Ge, As, Nb, Mo, Tc, Ru, Rh, Pd, Ag, Cd, In, Sn, and Sb). The removal time constant is set to 30 s with 100% efficiency; (2) an online chemical reprocessing system which removes soluble FPs from both fuel salt and fertile salt. In online chemical reprocessing, U, Np, and Pu are extracted by fluorination and returned first to the core. Then, most actinides including Th, Pa, and minor actinides (MA) are extracted by reductive extraction and stored in a stockpile for several months to let ^{233}Pa decay into ^{233}U. Finally, the carrier salt is recovered through low-pressure distillation, leaving the FPs for disposal.

3 Calculation tools

Here, an in-house program (TMCBurnup) which couples a problem-dependent cross-sectional processing module, a criticality analysis module in the SCALE6.1 program [18], and a novel depletion code MODEC was used for calculation [19]. SCALE6.1 is a comprehensive code package developed by ORNL, which is used to analyze criticality safety, radiation shielding design, sensitivity, etc. [18]. In an MSR, due to online reprocessing and refueling, the depletion equation can be described as follows:

$$\begin{cases} \dfrac{\mathrm{d}Ni(t)}{\mathrm{d}t} = \sum_j \lambda j, iNj(t) - \lambda iNi(t) + Ci \\ \lambda j, i = f_{j\to i}\sigma_j\phi(t) + \gamma_{j\to i}\lambda_j,\ \lambda_i = \sigma_i\phi(t) + \lambda_i + \lambda_i^c \end{cases} \quad (1)$$

where $N_i(t)$ and $N_j(t)$ refer to the number density of nuclide i and j, respectively; $\gamma_{j\to i}$ indicates the branching ratio of decay from nuclide j into i; λ_i and λ_j refer to the decay constant of nuclide i and j, respectively; $f_{j\to i}$ represents the probability of nuclide j to i by neutron absorption; λ_i^c indicates the fictive decay constant of nuclide i due to chemical reprocessing; σ_i and σ_j denote the absorption cross sections of nuclide i and j, respectively; and C_i refers to the feed rate of nuclide i. To solve this non-homogeneous equation, an in-house molten salt reactor-specific depletion code (MODEC) was developed in our previous work [18], which implemented two depletion algorithms to solve the depletion equation: the transmutation trajectory analysis (TTA) and the Chebyshev rational approximation method (CRAM). To simulate the online reprocessing, the fictive decay constant method was applied. Three methods were implemented in MODEC to solve the non-homogeneous burnup equation in the continuously refueling problems. In comparison with ORIGEN-S [20], the validity of MODEC in terms of the burnup calculations with online reprocessing and with continuous refueling was proved [21, 22].

A flowchart of TMCBurnup is shown in Fig. 3. The test results in MSFR show that the calculations using TMCBurnup agreed well with the reference values and were suitable for analyzing the Th–U cycle performance of MCFR and MFFR [21].

Due to the deep burnup of the molten salt reactor, the transition time from start-up to an equilibrium state is quite long, so the simulation of the entire burnup process would take longer. For some studies, only the equilibrium state analysis was needed. Therefore, MESA (molten salt reactor equilibrium state analysis code) [22], an in-house program, was used to quickly obtain the equilibrium state of the molten salt reactor; Table 2 shows the test results. The nuclide content, including that of the fission products and MA, could be found to be nearly the same as those calculated by TMCBurnup.

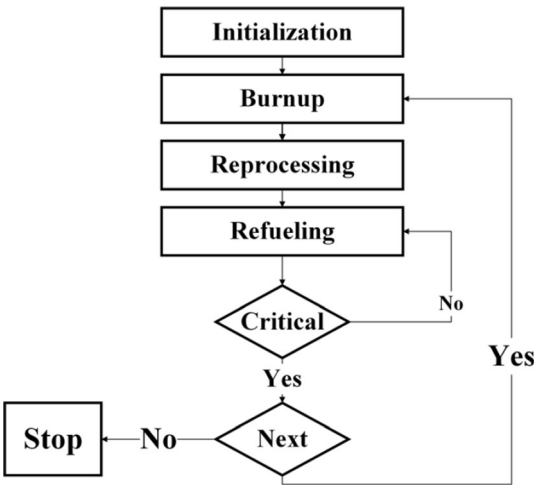

Fig. 3 Flowchart of TMCBurnup

4 Results and discussion

Here, the Th–U cycle performance of an MCFR and MFFR was investigated under a B&B scenario [23], in which some ^{233}U produced by the decay of the extracted ^{233}Pa needed to be refueled to the reactor to maintain criticality. Due to the lack of naturally available ^{233}U, high-assay low-enriched uranium (HALEU) and Pu elements produced by current LWRs were used as start-up fissile materials to achieve a transition to the Th–U cycle [24]. For the HALEU-started mode, the enrichment of ^{235}U was 19.75%; for Pu-started mode, it appeared more practical as it employed the prevailing PUREX reprocessing technique and facilities to recover Pu from LWRs. Initial nuclei inventories of the MFFR and MCFR with various fuel types are detailed in Table 3. For comparison, the ^{233}U-started case is also listed.

Here, the characteristics of the B&B thorium fuel cycle transition scenario in an MCFR and MFFR were studied based on several important parameters including neutron spectra, evolution of main heavy nuclides, breeding capacity, temperature coefficient of reactivity (TCR), delayed neutron fraction (β_{eff}), and radio-toxicity. A 238-group ENDF-B/VII.0 cross-sectional library was used in the calculation. In addition, there were 10,000 neutrons per k_{eff} cycle. We skipped the first 15 k_{eff} cycles to allow the spatial fission source to attain equilibrium, before the k_{eff} values were used for averaging for the final k_{eff} estimate. A total of 285 k_{eff} cycles were run in a criticality calculation with an average error of about 25 pcm.

4.1 Comparison of neutron spectra

Neutron spectra which could help fundamentally indicate subsequent interpretations of results based on the actinide buildup and TCR were researched here. Figure 4a shows the initial neutron spectra; those of the MCFR were harder than those of the MFFR, using either HALEU or Pu as start-up fissile materials, thanks to the larger relative atomic mass of NaCl as compared to LiF. It resulted in a weaker moderating ability in the MCFR. Moreover, due to the slowing of neutrons on the outer graphite besides the blanket, a peak appeared in the thermal spectrum zone in both the MFFR and MCFR.

Table 2 Heavy nuclide content at equilibrium state

Nuclides	TMCBurnup (460 years)	MESA	Relative deviation (%)
^{238}Pu	758.1356	763.8841	0.75
^{239}Pu	300.7233	302.7175	0.66
^{240}Pu	253.5638	255.2068	0.65
^{241}Pu	50.1238	51.2117	2.09
^{242}Pu	43.1527	44.1117	2.18
^{233}Pa	560.0238	564.0204	0.71
^{232}Th	223,732.3670	223,911.3605	0.08
^{232}U	52.5322	54.5737	3.73
^{233}U	20,147.4153	20,253.4150	0.52
^{234}U	10,468.3838	10,668.8636	1.87
^{235}U	2493.3333	2520.9230	1.08
^{237}Np	677.0324	697.0632	2.87
^{244}Cm	14.9982	15.1728	1.16
^{241}Am	11.9948	12.3778	3.09
^{243}Am	12.1382	12.4944	2.85
^{126}Sn	1579.7802	1598.7732	1.20
^{93}Zr	37,728.1378	37,739.5628	0.04
^{79}Se	589.5328	592.5327	0.49
^{90}Sr	21,037.1562	21,108.5632	0.34
^{137}Cs	9300.1377	9308.6855	0.09

Table 3 Initial nuclei inventories with various starting fuels (unit: g)

Nuclides	MFFR			MCFR		
	HALEU	Pu	^{233}U	HALEU	Pu	^{233}U
U-235	9.20E+06			7.68E+06		
U-238	3.73E+07			3.11E+07		
Pu-238		2.93E+05			1.77E+05	
Pu-239		8.51E+06			5.14E+06	
Pu-240		4.12E+06			2.49E+06	
Pu-241		5.92E+05			3.58E+05	
Pu-242		1.19E+06			7.18E+05	
Th-232	1.36E+07	4.52E+07	5.31E+07	1.18E+07	4.13E+07	4.44E+07
U-233			6.52E+06			5.20E+06
Total mass	6.02E+07	5.99E+07	5.97E+07	5.06E+07	5.02E+07	4.96E+07
Fissile isotope fraction	3.44%	3.42%	2.46%	6.84%	4.93%	4.69%

In order to quantitatively describe neutron spectra during the entire operation, the energy of the average lethargy causing fission (EALF) was introduced [25], which was used as a quantization parameter of the average neutron energy in a reactor expressed as:

$$\mathrm{EALF} = \exp\left\{\frac{\int (\ln E)\phi(E)\sum_f (E)\mathrm{d}E}{\int \phi(E)\sum_f (E)\mathrm{d}E}\right\}, \quad (2)$$

where $\phi(E)$ and $\Sigma_f(E)$ represent the energy-dependent neutron flux and macroscopic fission cross section, respectively. The higher the value of EALF, the harder the neutron spectrum. Figure 4b shows the evolution of EALF. Neutron spectra of the MCFR were found to be harder than that of MFFR during the entire operation. In addition, neutron spectra of the Pu-started mode were harder than that of the HALEU-started mode, initially. Moreover, due to the accumulation of FPs during the operation, EALF gradually decreased except for that of the HALEU-started mode in the MFFR, resulting from its relatively lighter atomic mass than that of the fissile and fertile nuclides, bringing about a stronger moderating effect on the neutrons. For the HALEU-started mode in the MFFR, EALF of the LEU-started mode increased slightly in the first few years due to a decrease in ^{238}U; it had a broader resonance

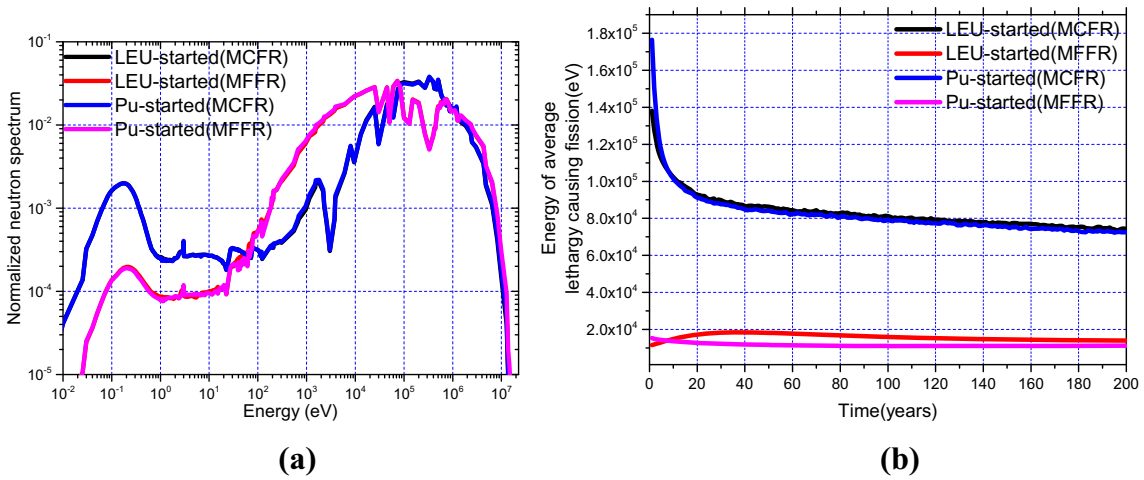

Fig. 4 (Color online) Neutron spectra at initial time (**a**) and the evolution of EALF (**b**)

peak and a larger resonance capture cross section than ^{232}Th, resulting in a more obvious resonance in the neutron spectra. Then, it gradually attained an equilibrium state on consumption of ^{238}U and buildup of FPs.

4.2 Breeding capability

Here, the breeding performance of an MFFR and MCFR were explored based on the breeding ratio (BR), net production of ^{233}U, and doubling time (DT), the three important parameters for evaluating fuel breeding performance. BR, which represents the ratio of the capture rates of all fertile isotopes and the absorption rate of all fissile isotopes, is expressed by Eq. (3). During the operation, ^{233}Pa was extracted from the core and blanket, and stored outside the reactor to let it decay into ^{233}U. To maintain criticality, some ^{233}U needed to be fed back into the core; the amount of remaining ^{233}U outside the reactor is the net ^{233}U production. When the mass of ^{233}U outside the reactor equaled that at initial ^{233}U loading, it indicated that the produced ^{233}U was sufficient to start a new MCFR/MFFR. DT is the time required to double the amount of ^{233}U [26].

$$\mathrm{BR} = \frac{Rc(^{234}\mathrm{U} + ^{232}\mathrm{Th} + ^{240}\mathrm{Pu} + ^{238}\mathrm{U}) - Ra(^{233}\mathrm{Pa})}{Ra(^{233}\mathrm{U} + ^{235}\mathrm{U} + ^{241}\mathrm{Pu} + ^{239}\mathrm{Pu})}, \quad (3)$$

where R_c indicates the neutron capture reaction rate of fertile isotopes and R_a denotes the neutron absorption reaction rate of fissile nuclides. Firstly, MESA was used to investigate the BR of an MCFR and MFFR in equilibrium state at varying reprocessing rates. The results are shown in Fig. 5. At the same reprocessing rate, the BR in an MCFR was higher than that in an MFFR at an equilibrium state. As the reprocessing rate reached 3.25 L/day, the BR of an MCFR equaled 1, suggesting that it could be self-sustaining at that reprocessing rate, while an MFFR became self-sustaining as the reprocessing rate increased to 9.6 L/day. As the reprocessing rate increased to 200 L/day, the BR of an MFFR and MCFR was 1.12 and 1.31, respectively.

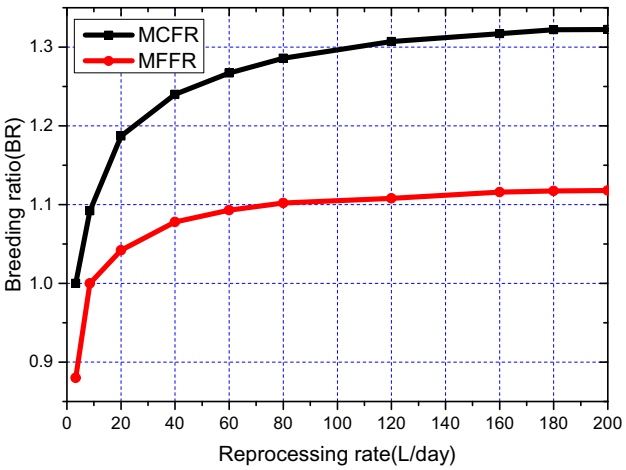

Fig. 5 (Color online) BR of an MCFR and MFFR in an equilibrium state versus reprocessing rate

As the online reprocessing of fast reactors, especially that of Th–U–Pu mixed fast reactors is challenging, a reprocessing rate of 40 L/day was selected for the subsequent calculation [1]. A 200-year burnup was simulated here, as it takes longer for some neutron parameters in molten fast reactors to reach an equilibrium state, which include delayed neutron fraction (β_{eff}), mass of actinides, as well as the BR [5, 24]. It involves many fertile and fission nuclides in the initial stage when using Pu or LEU as start-up fissile materials, so as to express the relationship between ^{233}U generation and direct disappearance. Regeneration ratio (RR) is defined by Eq. (4); an RR

greater than 1 suggests that the production of ^{233}U is greater than its consumption.

$$\mathrm{RR} = \frac{Rc(^{232}\mathrm{Th}) - Ra(^{233}\mathrm{Pa})}{Ra(^{233}\mathrm{U})}. \quad (4)$$

Figure 6a shows the evolution of k_{eff} and RR during the reactor operation. During the entire operation, k_{eff} was maintained between 1.000 and 1.005, while RR decreased in the early years, gradually tending to an equilibrium state. This mainly occurred as the core maintains its criticality by consuming ^{239}Pu and ^{235}U in the early stage; the consumption of ^{233}U is small. As ^{233}U gradually becomes the dominating fissile isotope, its consumption rate increases, leading to a decrease in the RR. In addition, due to the harder neutron spectra in an MCFR, its capture-to-fission ratio (α) is smaller, resulting in an obviously larger RR throughout the operation. The evolution of net production of ^{233}U is shown in Fig. 6b; the dashed line represents the initial ^{233}U inventories, using ^{233}U as the start-up fissile material. A higher RR in an MCFR resulted in a faster net accumulation of ^{233}U. The DT of HALEU-started and Pu-started modes in an MFFR and MCFR was 88.0 and 48.0 years, and 16.5 years and 16.2 years, respectively. For comparison, the DT of an MSCFR which used NaCl as a carrier salt was 17 years, while that of an MSFR using LiF as a carrier salt was 56 years in the TRU-started mode [24, 27]. Besides, at the equilibrium state, the average annual net production of ^{233}U for an MCFR and MFFR was 243 kg and 86 kg, respectively.

4.3 Evolution of heavy nuclides

The evolution of heavy nuclides and U isotopes for an MFFR and MCFR initiated with Pu and HALEU is presented in Figs. 7a, b and 8a, b, and provides an important basis for analyzing core critical performance and nuclear waste production. Despite an equilibrium state determined by the feeding fuel composition, some different features in the transition state with the same feeding fuel still exist. Achieving equilibrium of heavy nuclides in an MCFR is more time-consuming due to its harder neutron spectrum. Moreover, for the Pu-started mode, fewer neutrons need to be absorbed to reach equilibrium; hence, the time required to reach equilibrium is shorter than that for the HALEU-started mode. Although the total mass of U isotopes is larger in an MCFR than MFFR, the ^{232}U content of an MCFR is always higher than that of an MFFR throughout the operation. This is because the generation of ^{232}U mainly relies on the (n, $2n$) reaction of ^{233}U [28]; the reaction cross section increases with the hardening of the neutron spectrum. As is well known, ^{232}U decay chains contain a number of highly radioactive decay products, particularly ^{208}Tl, which emits gamma rays of up to 2.6 MeV, increasing the nonproliferation capacity of an MCFR.

The molar ratio of U isotopes in the blanket at equilibrium state is shown in Table 4. It indicates that the purity of ^{233}U is considerably high with the molar ratio for an MCFR and MFFR being 95.28% and 99.22%, respectively. Importantly, the ^{232}U content for an MCFR and MFFR is only 6 ppm and 0.03 ppm, respectively. Thus, nuclear proliferation issues could arise, ^{233}U being easily retrievable through fluorination from the blanket.

4.4 Safety parameters

TCR and β_{eff} are important parameters that could provide insights on the safety and relative potential for various modes. In one-group approximation, k_{eff} can be expressed as:

$$k_{\mathrm{eff}} = \frac{k_\infty}{1 + B^2 L^2}, \quad (5)$$

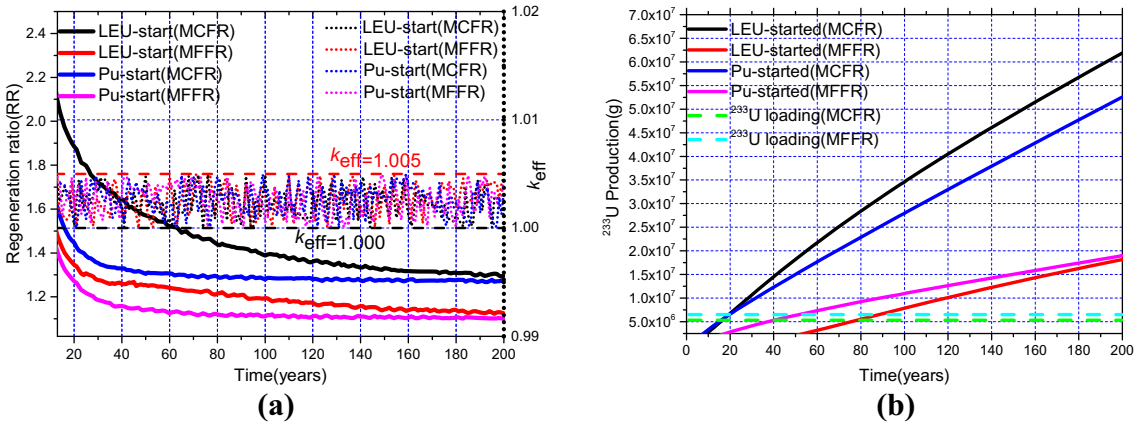

Fig. 6 Evolution of the RR (**a**) and net production of ^{233}U (**b**)

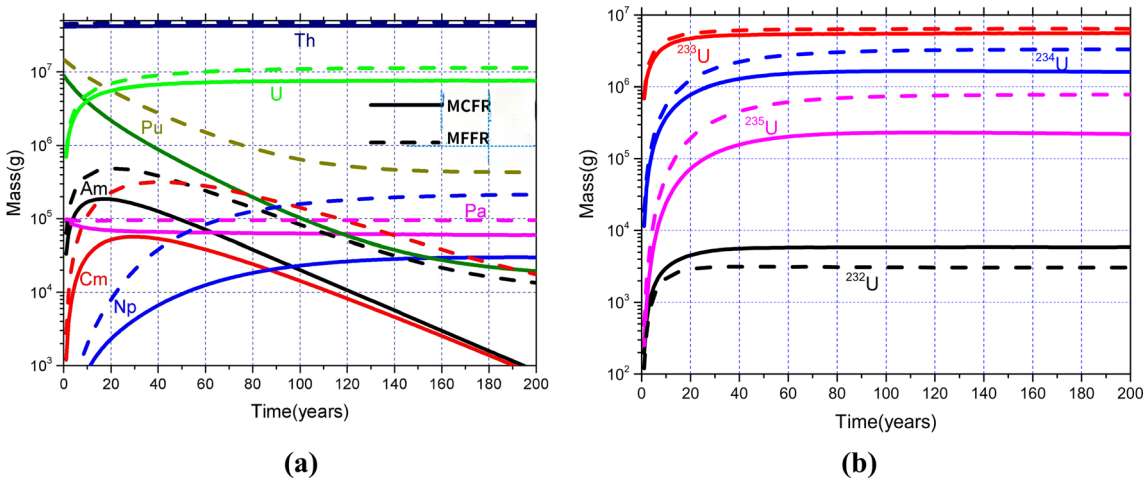

Fig. 7 (Color online) Evolution of heavy nuclides (**a**) and U isotopes (**b**) for an MFFR and MCFR started with Pu

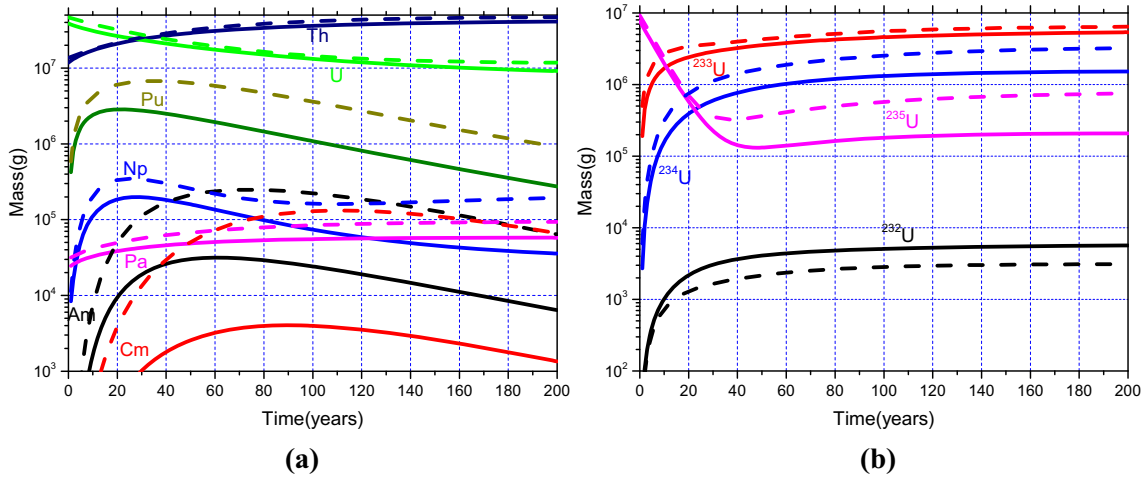

Fig. 8 (Color online) Evolution of heavy nuclides (**a**) and U (**b**) isotopes started with HALEU

Table 4 Molar ratio of U isotopes at equilibrium (%)

Nuclides	MCFR	MFFR
^{232}U	0.13	3.74E−3
^{233}U	95.28	99.22
^{234}U	4.24	0.77
^{235}U	0.35	0.01

where k_∞ refers to infinite multiplication; B represents buckling; and L stands for diffusion length. TCR is mainly determined by the effect of the fuel density and Doppler coefficient; the Doppler effect which is paramount to TCR acts on the k_{eff}. For a molten salt fast reactor, an increasing temperature contributes negatively to reactivity due to an increased capture of fertile isotopes in the region of resonance. In general, the impact of the Doppler effect will weaken with local spectrum hardening; hence, the absolute value of the Doppler coefficient in an MFFR is larger.

Moreover, a second reactivity feedback depends on fuel expansion and impacts the term L^2 along with the Doppler effect, simultaneously. In one-group approximation, L^2 is defined as:

$$L^2 = \frac{D}{\sum_{\text{a}}} \propto \frac{1}{d^2}, \tag{6}$$

where d represents the density of the fuel salt; D is the diffusion coefficient; and $\sum_{\text{a}}$ indicates the macroscopic absorption cross section. Density decreases with an increase in temperature, resulting in a negative feedback coefficient.

While B^2 is mainly caused by the expansion of the core structure, and the feedback coefficient is clearly positive, the expansion coefficient of the structure is much lower than that of the salt. Besides, during a transient, the fuel salt undergoes quick temperature excursions, while a much slower temperature variation is expected from the core structure; thus, this effect can be ignored. Due to the

absence of a moderator in an MCFR and MFFR, TCR can be expressed as:

$$\left(\frac{\mathrm{d}K}{\mathrm{d}T}\right)\text{total} = \left(\frac{\mathrm{d}K}{\mathrm{d}T}\right)\text{fuel Doppler} + \left(\frac{\mathrm{d}K}{\mathrm{d}T}\right)\text{fuel density}, \tag{7}$$

where K and T indicate the k_{eff} and temperature, respectively. Figure 9 shows the evolution of TCR for the four Th–U cycle modes. Initially, the TCR of the four Th–U cycle modes was noticeably different; the absolute TCR value of an MCFR was larger than that of an MFFR due to a considerably higher expansion coefficient in molten chloride salt. Moreover, the Pu-started mode demonstrated a higher absolute TCR value than the HALEU-started mode at initial time, while the absolute TCR values of the Pu-started and HALEU-started modes were the same at equilibrium.

The Doppler effect is mainly driven by resonance captures in the fertile isotopes. The spectrum shift ensues increased fertile captures affecting fission and capture in other isotopes, while the fuel density effect is mainly driven by leakages, which depend only mildly on the fuel composition; the tendency is similarly to the Doppler coefficient. Due to the lower molar fraction of fertile isotopes in the HALEU start-up mode, the absolute TCR value was initially smaller. With the operation, the nuclide composition in an MCFR/MFFR tends to be the same, which leads to the TCR becoming gradually identical. Moreover, the dominant fissile isotope in the Pu-started mode (^{239}Pu, ^{235}U) has a flatter fission cross section than ^{233}U. Thus, spectral hardening has a less negative impact on ^{239}Pu and ^{235}U fission rather than on ^{233}U. In addition, ^{239}Pu and ^{235}U also have a steeper capture cross section as compared to ^{233}U, suggesting a higher decrease in captures following spectral hardening, positively affecting TCR [2].

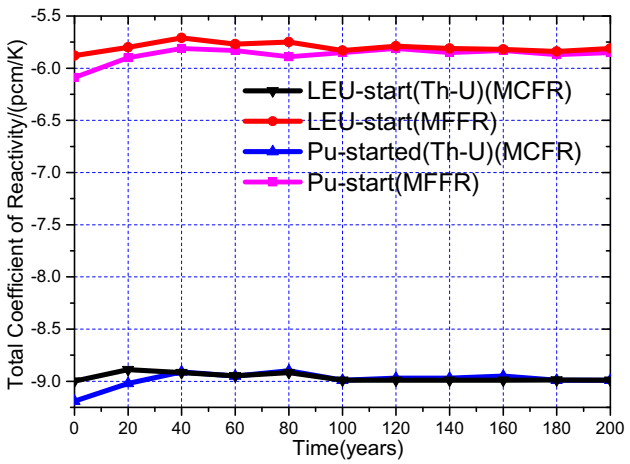

Fig. 9 (Color online) Evolution of TCR for different modes

Therefore, a high ^{233}U content is beneficial for the Doppler coefficient.

Although ^{233}U gradually becomes the dominant fissile isotope under the operation, TCR fluctuates slightly due to the buildup of FPs. The spectrum hardening following a temperature increase leads to a decrease in FP captures; thus, a higher FP content suggests a higher decrease in FP captures with spectrum hardening, which leads to increased reactivity, positively affecting TCR.

In addition, β_{eff} is extremely important for reactor operation control, which is primarily determined by the fission rate fraction and the single delayed neutron fraction of fissile isotopes (Table 5). It can be expressed as:

$$\beta\text{eff} = \frac{\sum_i \overline{vd}(i) \cdot Rf(i)}{\sum_i (\overline{vd}(i) + \overline{vp}(i)) \cdot Rf(i)}, \tag{8}$$

where $vd(i)$ and $vp(i)$ represent the delayed neutron number and prompt neutron number per fission for nuclide i, respectively, and $Rf(i)$ denotes the neutron fission rate for nuclide i. Table 5 shows the single β_{eff} of various fissile isotopes. Due to the non-negligible fission cross section of ^{234}U in the fast spectrum, the fission contribution of ^{234}U was also considered. The evolution of the total β_{eff} of different modes is displayed in Fig. 10.

In HALEU-started modes, the total β_{eff} dropped rapidly in the first few decades; then, it increased slightly and gradually transitioned to an equilibrium state. A rapid decline in β_{eff} is primarily due to a decrease in the fission rate fraction of the dominant fissile isotope ^{235}U, while that of other fissile isotopes, especially ^{233}U, increased (Fig. 11). After the first 20 years, with the depletion of ^{239}Pu, the total β_{eff} gradually increased and then tended to be constant. As for Pu-started modes, with ^{239}Pu gradually replaced by ^{233}U, the total β_{eff} gradually increased and then tended to be constant at 291 pcm and 312 pcm in an MCFR and MFFR, respectively. Moreover, due to the higher fission rate fraction of ^{234}U in an MFFR (Fig. 11), the total β_{eff} at equilibrium state was higher than that of an MCFR. Throughout the operation, the changes of total β_{eff} in an MCFR and MFFR for the HALEU-started and Pu-started

Table 5 Delayed neutron fraction for various isotopes for an MCFR and MFFR

Fissile isotopes	MFFR (pcm)	MCFR (pcm)
^{233}U	292	291
^{234}U	535	532
^{235}U	662	668
^{239}Pu	219	218
^{241}Pu	544	542

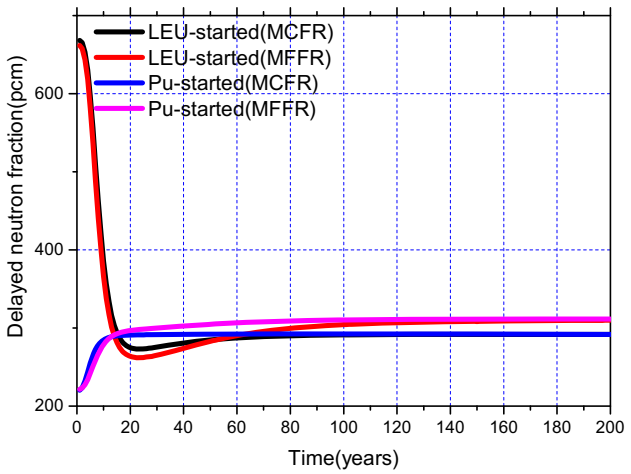

Fig. 10 (Color online) Evolution of total β_{eff} of different modes

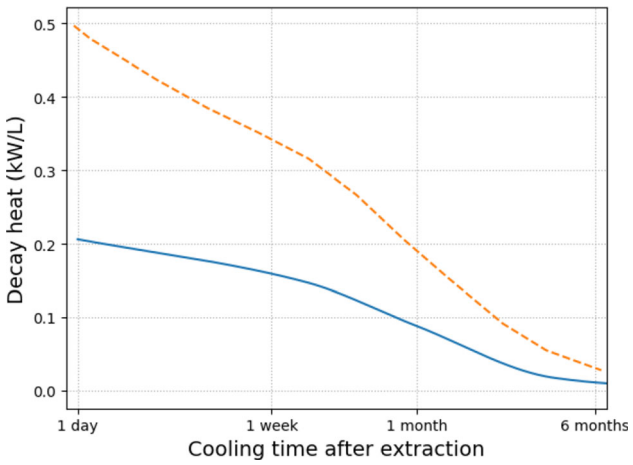

Fig. 12 Evolution of decay heat of fuel salt for an MCFR (solid line) and MFFR (dashed line)

modes were 369 pcm and 62 pcm; and 335 pcm and 89 pcm, respectively.

4.5 Radioactivity analysis

Radioactivity analysis is an important aspect of reactor safety analysis. Here, the radioactivity of the fuel salt in an MCFR and MFFR was analyzed to provide a reference for the radiation shielding design during online reprocessing. Thereafter, the radioactivity of the nuclear waste was analyzed to provide relevant parameters for the intermediate storage and final repository of nuclear waste.

Online reprocessing leads to a good breeding performance and neutron economy of an MSR, but at the cost of facing the highly radioactive fuel salt throughout the operation. In order to be sure of the radiation shielding design and fuel salt cooling time, the radioactivity of the fuel salt in an MCFR and MFFR was analyzed.

Figure 12 shows the evolution of the decay heat of fuel salt during reprocessing. Due to a lower content of the short-lived FPs (^{137}Cs and ^{90}Sr, about 30-year half-life) at equilibrium state (Fig. 13), the decay heat in an MCFR is much lower than that in an MFFR; it drops to a negligible level much faster. Figure 14 shows the evolution of high-energy gamma radiation; the horizontal dashed line denotes the high-energy gamma-ray level of the spent fuel in a sodium-cooled fast reactor, which has been cooling for 5 years [29]. The high-energy gamma-ray level of an MCFR was also found to be lower than that of an MFFR, and its value dropped to the reference level within three months; however, it took over 2 years in an MFFR to drop to reference level.

Due to the specificity of neutron shielding, it is necessary to calculate neutron emissions in a fuel salt during reprocessing. Figure 15 shows the evolution of neutron emissions. The neutron emission rate of an MCFR was

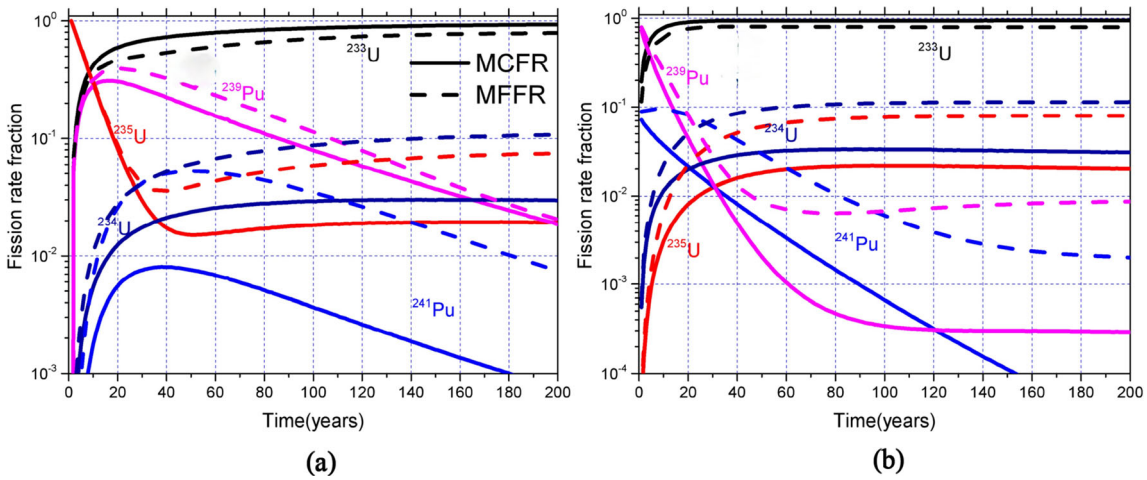

Fig. 11 (Color online) Evolution of fission rate fraction with **a** HALEU, and **b** Pu as start-up materials

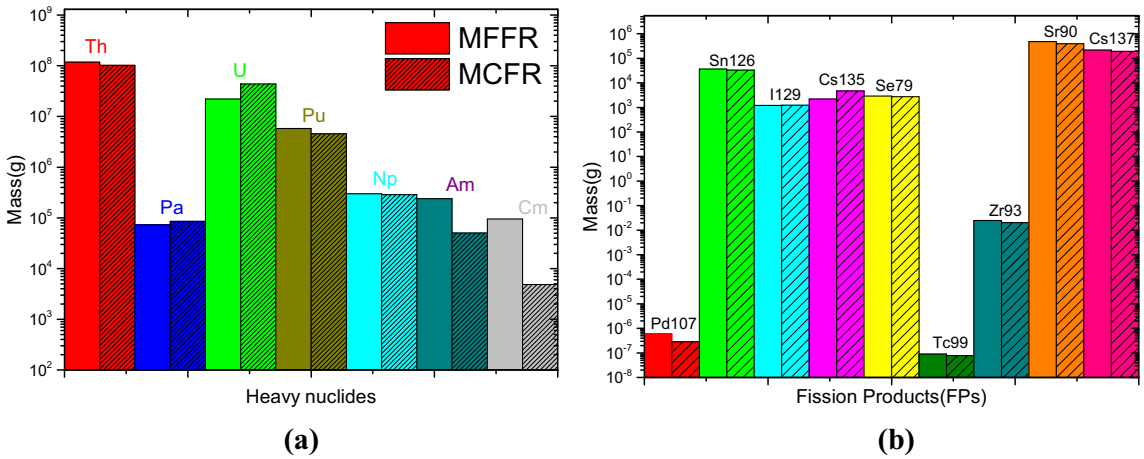

Fig. 13 (Color online) Mass of heavy nuclides (**a**) and FPs (**b**) at equilibrium state

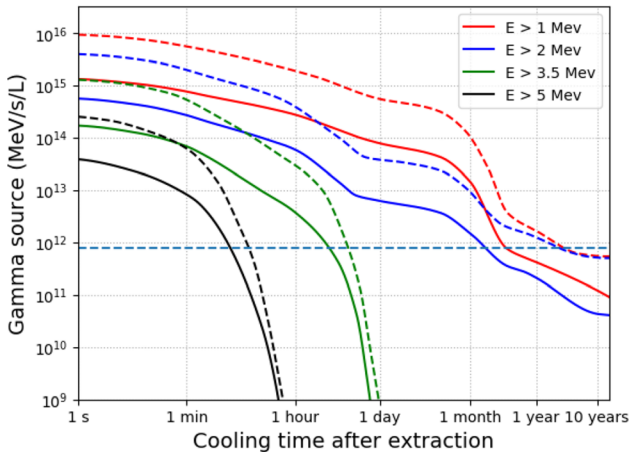

Fig. 14 (Color online) Evolution of high-energy gamma radiation for an MCFR (solid line) and MFFR (dashed line)

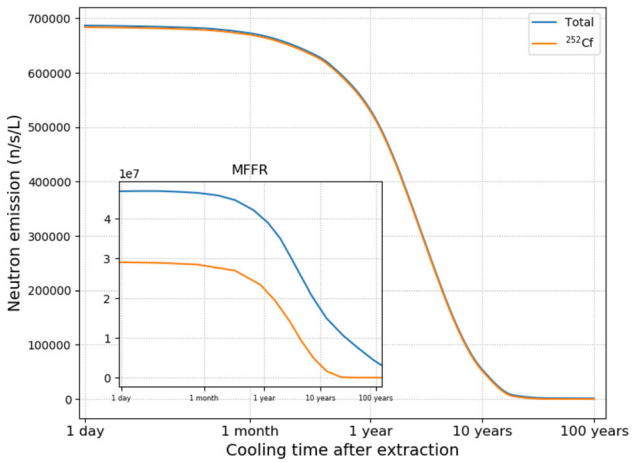

Fig. 15 (Color online) Evolution of neutron emissions for an MCFR and MFFR

only 1/60th that of an MFFR, with almost all originating from the spontaneous fission of ^{252}Cf, resulting from a higher content of heavy nuclides in an MFFR due to its softer neutron spectrum.

Radio-toxicity and decay heat derived from nuclear waste have a non-negligible impact on reprocessing, manufacturing, and particularly, on the final repository. For a closed cycle, all actinides need to be disposed only when the reactor is decommissioned. Therefore, the radio-toxicity and decay heat during operation are mainly derived from FPs during online reprocessing. Besides, a loss of nuclides occurs during online reprocessing; here, we assume a loss rate of 10^{-5} for TRU and 10^{-7} for uranium isotopes [30]; these nuclides are also the source of radio-toxicity and decay heat. Figure 16 shows the evolution of decay heat and radio-toxicity of nuclear waste.

It can be seen that the radio-toxicity and decay heat are mainly determined by FPs, while that generated by nuclear waste in an MFFR is slightly higher due to its higher FP content. The radio-toxicity of both an MCFR and MFFR dropped to the radioactivity level of natural uranium ore in 300 years. In addition, due to the buildup of highly radioactive daughter nuclei of ^{237}Np ($T_{1/2} = 2.14 \times 10^6$ years) and ^{233}U ($T_{1/2} = 1.59 \times 10^5$ years) such as ^{229}Th and ^{225}Ac, the second peak of the radio-toxicity and decay heat of TRU and U appeared at about 10^5 years.

5 Conclusion

In view of their good breeding performance, high inherent safety, and simple reprocessing requirements, molten salt fast reactors could be considered as ideal reactors for a closed Th–U cycle. This work focused on an investigation and comparison of the Th–U cycle performance of two typical types, i.e., MCFR and MFFR, using a computing tool developed in-house. Important parameters, including the evolution of heavy nuclides, breeding

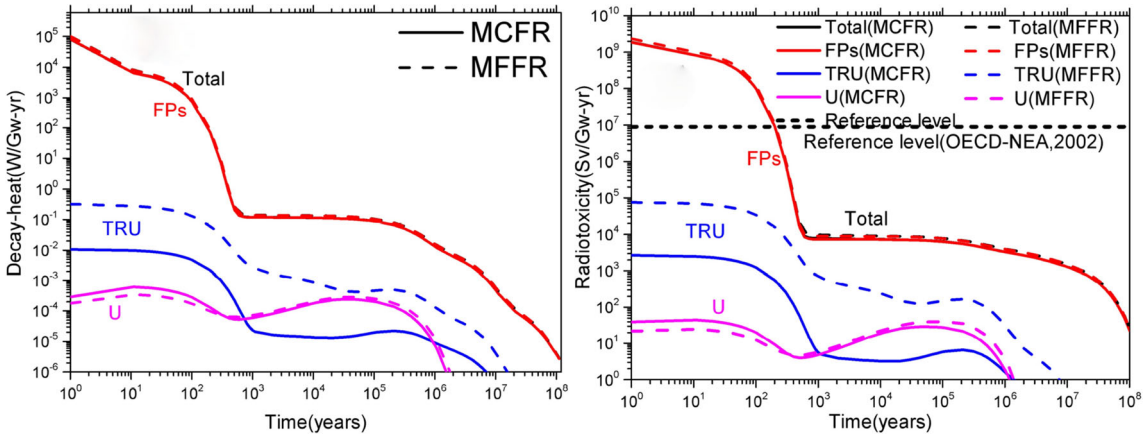

Fig. 16 Evolution of **a** Decay heat and **b** radio-toxicity of nuclear waste

capability, safety parameters, and radio-toxicity were investigated and discussed to understand the transition behavior throughout the operation. It can be concluded that:

(1) Regardless of HALEU or Pu being used as start-up fuels, the initial loading fissile nuclides of an MFFR are heavier than that of an MCFR. An MCFR could become self-sustaining at a reprocessing rate of 3.25 L/day, and an MSFR at 9.6 L/day. At a reprocessing rate of 40 L/day, the DT of an MCFR and MFFR in HALEU-started mode and Pu-started mode was 16.5 and 16.2 years; and 88.0 and 48.0 years, respectively. Moreover, the average ^{233}U production at equilibrium state for an MCFR and MFFR was 243 kg and 86 kg, respectively.

(2) Throughout the operation, TCR was sufficiently negative in an MCFR and MFFR, and the absolute value of TCR in an MCFR was higher due to its obvious fuel density coefficient. In addition, the delayed neutron fraction in the HALEU-started mode dropped more than 330 pcm in both an MCFR and MFFR, while in an MFFR it had a smaller fluctuation and was about 30 pcm higher than that of an MCFR at equilibrium state.

(3) Due to the heavier initial critical loading of fissile nuclides and the softer energy spectrum, the TRU and FP content in an MFFR was higher, which leads to a stronger high-energy gamma radiation, higher neutron emission rate and decay heat in the fuel salt, as well as higher radio-toxicity and decay heat in the nuclear waste. It proposes a greater requirement for radiation shielding design and nuclear waste management during reprocessing.

References

1. D. Heuer, E. Merle-Lucotte, M. Allibert et al., Towards the thorium fuel cycle with molten salt fast reactors. Ann. Nucl. Energy **64**, 421–429 (2014). https://doi.org/10.1016/j.anucene.2013.08.002
2. C. Fiorina, M. Aufiero, A. Cammi et al., Investigation of the MSFR core physics and fuel cycle characteristics. Prog. Nucl. Energy **68**, 153–168 (2013). https://doi.org/10.1016/j.pnucene.2013.06.006
3. C. Fiorina, D. Lathouwers, M. Aufiero et al., Modelling and analysis of the MSFR transient behavior. Ann. Nucl. Energy **64**(2), 485–498 (2014). https://doi.org/10.1016/j.anucene.2013.08.003
4. V. Ignatiev, F. Olga, G. Ivan et al., Progress in development of Li, Be, Na/F molten salt actinide recycler & transmutation concept. ICAPP (2017)
5. E. Merle-Lucotte, D. Heuer, M. Allibert et al. The thorium molten salt reactor: Launching the thorium fuel cycle with the molten salt fast reactor. ICAPP (2011)
6. GIF (Generation IV International Forum) Annual Report 2008(2008), pp. 36–41. http://www.gen-4.org/PDFs/GIF_2008_Annual_Report.pdf
7. J.J. Bulmer, E.H. Gift, R.J. Holl et al., *Reactor design and feasibility study: fused salt fast breeder* (Oak Ridge School of Reactor Technology, Oak Ridge, 1956)
8. L.Y. He, S.P. Xia, R. Yan et al., Th–U and U–Pu cycling performances of molten chloride salt fast reactor under LEU start-up mode. Nucl. Tech. **43**(1), 010604 (2020). https://doi.org/10.11889/j.0253-3219.2020.hjs.43.010604. **(in Chinese)**
9. J. Smith, W.E. Simmons, *An assessment of a 2500 MWe molten chloride salt fast reactor* (United Kingdom Energy Authority Reactor Group, Winfrith, 1974)
10. I. Scott, T. Abram, Stable salt reactor design concept. Proceedings of the International Thorium Energy Conference: Gateway to Thorium Energy (2015)
11. A. Huke, G. Ruprecht, D. Weißbach et al., The dual fluid reactor—a novel concept for a fast nuclear reactor of high efficiency. Ann. Nucl. Energy **80**, 225–235 (2015). https://doi.org/10.1016/j.anucene.2015.02.016
12. L.Y. He, Y. Zou, R. Yan et al. Design optimization and burnup analysis for molten chloride fast reactor. ICAPP (2020)
13. A. Mourogov, P.M. Bokov, Potentialities of the fast spectrum molten salt reactor concept: REBUS-3700. Energy Convers. Manag. **47**(17), 2761–2771 (2006). https://doi.org/10.1016/j.enconman.2006.02.013

14. A. Nuttin, D. Heuer, A. Billebaud et al., Potential of thorium molten salt reactors detailed calculations and concept evolution with a view to large scale energy production. Prog. Nucl. Energy **46**(1), 77–99 (2005). https://doi.org/10.1016/j.pnucene.2004.11.001
15. G.C. Li, Y. Zou, C.G. Yu et al., Model optimization and analysis of Th–U breeding based on MSFR. Nucl. Tech. **40**(02), 020603 (2017). https://doi.org/10.11889/j.0253-3219.2017.hjs.40.020603. **(in Chinese)**
16. G.C. Li, Y. Zou, C.G. Yu et al., Influences of 7Li enrichment on Th–U fuel breeding for an improved molten salt fast reactor (IMSFR). Nucl. Sci. Tech. **28**, 97 (2017). https://doi.org/10.1007/s41365-017-0250-7
17. Y.P. Peng, C.G. Yu, D.Y. Cui et al., Analysis of burnup performance for a molten chloride salt fast reactor based on thorium fuel. Nucl. Tech. **41**(7), 070602 (2018). https://doi.org/10.11889/j.0253-3219.2018.hjs.41.070602. **(in Chinese)**
18. S.M. Bowman, Scale 6: comprehensive nuclear safety analysis code system. Nucl. Tech. **174**(2), 126–148 (2011). https://doi.org/10.13182/NT10-163
19. S.P. Xia, J.G. Chen, J.H. Wu et al., Development of a Molten Salt Reactor specifific depletion code MODEC. Ann. Nucl. Energy **124**, 88–97 (2019). https://doi.org/10.1016/j.anucene.2018.09.032
20. I. Gauld, *Origen-s: Depletion Module to Calculate Neutron Activation, Actinide Transmutation, Fission Product Generation, and Radiation Source Terms* (Oak Ridge National Laboratory, Oak Ridge, 2011)
21. L.Y. He, G.C. Li, S.P. Xia et al., Effect of ^{37}Cl enrichment on neutrons in a molten chloride salt fast reactor. Nucl. Sci. Tech. **31**, 27 (2020). https://doi.org/10.1007/s41365-020-0740-x
22. S.P. Xia, Research on the High-precision Burnup Calculation Methods and Thorium–Uranium Fuel Breeding For The Liquid-Fueled Molten Salt Reactors. University of Chinese Academy of Sciences (2019)
23. D.Y. Cui, S.P. Xia, X.X. Li et al., Transition toward thorium fuel cycle in a molten salt reactor by using plutonium. Nucl. Sci. Tech. **28**, 152 (2017). https://doi.org/10.1007/s41365-017-0303-y
24. E. Merle-Lucotte, D. Heuer, C. Brun et al., Fast thorium molten salt reactors started with plutonium. ICAPP (2006)
25. D.Y. Cui, X.X. Li, S.P. Xia et al., Possible scenarios for the transition to thorium fuel cycle in molten salt reactor by using enriched uranium. Prog. Nucl. Energy **104**, 75–84 (2018). https://doi.org/10.1016/j.pnucene.2017.09.003
26. C.G. Yu, X.X. Li, X.Z. Cai et al., Minor actinide incineration and Th–U breeding in a small FLiNaK molten salt fast reactor. Ann. Nucl. Energy **99**, 335–344 (2017). https://doi.org/10.1016/j.anucene.2016.09.025
27. A. Rykhlevskii, A. Worrall, K. Huff, Fuel cycle performance of fast spectrum molten salt reactor designs. M&C (2019)
28. E.I. Vapirev, V.I. Dimitrov, T.J. Jordanov et al., Conversion of high enriched uranium in thorium-232-based oxide fuel for light and heavy water reactors: MOX-T fuel. Nucl. Eng. Des. **167**(2), 105–112 (1996). https://doi.org/10.1016/S0029-5493(96)01285-X
29. S.J. Piet, S.E. Bays, Mi.A. Pope et al., Sustained Recycle in Light Water and Sodium-Cooled Reactors. United States: N. p., 2010. Web. (2010)
30. M. Aufiero, B. Mariya, C. Antonio et al., Calculating the effective delayed neutron fraction in the Molten Salt Fast Reactor: analytical, deterministic and Monte Carlo approaches. Ann. Nucl. Energy **65**, 78–90 (2014). https://doi.org/10.1016/j.anucene.2013.10.015